Journal of Neuroscience Methods 192 (2010) 102–109

Contents lists available at ScienceDirect

Journal of Neuroscience Methods

journal homepage: www.elsevier.com/locate/jneumeth

A three-dimensional digital segmented and deformable brain atlas of the domestic pig

Stéphan Saikali[a,*], Paul Meurice[b], Paul Sauleau[c], Pierre-Antoine Eliat[d], Pascale Bellaud[e], Gwenaelle Randuineau[b], Marc Vérin[f], Charles-Henri Malbert[b]

[a] Département d'Anatomie et Cytologie Pathologiques, CHU Pontchaillou, 2 rue Henri Le Guilloux, 35033 Rennes Cedex 09, France
[b] UMR SENAH, INRA, 35590 Saint-Gilles, France
[c] Service des Explorations Fonctionnelles Neurologiques, CHU Pontchaillou, 2 rue Henri Le Guilloux, 35033 Rennes Cedex 09, France
[d] PRISM-Villejean - IFR 140 – OUEST-génopôle, Université de Rennes 1, Campus de Villejean, CS 34317, 35043 Rennes Cedex, France
[e] Plate-forme Histo-Pathologie, IFR 140, Université de Rennes 1, Faculté de Médecine, 35043 Rennes Cedex, France
[f] Clinique Neurologique, Unité de Recherche Universitaire "Comportement et Noyaux Gris Centraux", CHU de Rennes, Hôpital Pontchaillou, Rue Henri Le Guilloux, 35033 Rennes Cedex 09, France

ARTICLE INFO

Article history:
Received 23 June 2010
Received in revised form 27 July 2010
Accepted 28 July 2010

Keywords:
Cytoarchitecture
MRI
Atlas
Stereotaxic
Histology

ABSTRACT

We used high-magnetic field (4.7 T) magnetic resonance imaging (MRI) to build the first high-resolution (100 μm × 150 μm × 100 μm) three-dimensional (3D) digital atlas in stereotaxic coordinates of the brain of a female domestic pig (*Sus scrofa domesticus*).

This atlas was constructed from one hemisphere which underwent a symmetrical transformation through the midsagittal plane. Concomitant construction of a 3D histological atlas based on the same scheme facilitated control of deep brain structure delimitation and enabled cortical mapping to be achieved. The atlas contains 178 individual cerebral structures including 42 paired and 9 single deep brain structures, 5 ventricular system areas, 6 paired deep cerebellar nuclei, 12 cerebellar lobules and 28 cortical areas per hemisphere. Given the increasing importance of pig brains in medical research, this atlas should be a useful tool for intersubject normalization in anatomical imaging as well as for precisely localizing brain areas in functional MR studies or electrode implantation trials.

The atlas can be freely downloaded from our institution's Website.

1. Introduction

The domestic pig is a common animal model for human digestive and nutritional physiology (Malbert and Horowitz, 1997; Spurlock and Gabler, 2008). We recently note that this animal model is increasingly being used in the field of neuroscience, particularly for studying pharmacological drugs and for developing pathological models dealing with traumatic brain injury, stroke or poisoning induced neurodegenerative diseases (Lind et al., 2007). The pig brain is gyrencephalic and resembles the human brain in anatomy and development more than the brain of small commonly used laboratory animals (Lind et al., 2007). Its size allows multimodality imaging and facilitates surgical procedures and electrode installation, making the pig a useful animal model in deep brain stimulation (DBS) trials (Sauleau et al., 2009).

Neuronavigation and functional imaging require a reliable stereotaxic atlas of the pig brain allowing its warp to fit each animal's unique anatomy and being available for multimodality imaging. To date, the sole available stereotaxic atlas of a domestic pig brain is structured from histological slice drawings (Felix et al., 1999). This atlas presents numerous shifts in orthogonal reslicing of the drawings, leading to many inaccuracies in the spatial localization of brain areas. Furthermore, the major limitation of this printed atlas relates to its difficulty in mapping the printed information onto an individual brain.

The aim of our work was to construct a detailed and sufficiently accurate digital atlas accessible to multimodality imaging.

This atlas was constructed from high-resolution MR images and their corresponding histological slices of one hemisphere which underwent a symmetrical transformation through the midsagittal plane leading to a virtual MRI and histological volume. The high-resolution of the MR images (100 μm × 150 μm × 100 μm) facilitated recognition and manual delineation of the majority of the identified deep brain structures. Histological slices facilitated the control of deep brain structure delimitation and allowed cortical mapping to be achieved.

Abbreviations: MRI, magnetic resonance imaging; 3D, three-dimensional; DBS, deep brain stimulation; ROI, region of interest; VOI, volume of interest.

* Corresponding author: Tel.: +33 02 99 28 42 79; fax: +33 02 99 28 42 84.
E-mail address: stephan.saikali@chu-rennes.fr (S. Saikali).

0165-0270/$ – see front matter © 2010 Elsevier B.V. All rights reserved.
doi:10.1016/j.jneumeth.2010.07.041

This construction and delineation process was used to build a high-resolution 3D digital atlas in stereotaxic coordinates of a domestic pig brain, a tool which offers more visualization facilities and computational power than conventional 2D paper atlases.

This atlas can be used for functional brain mapping studies and functional surgery with specific reference to cortical stimulation, and reduces the statistical variability due to type I errors in functional brain imaging studies using an ROI (Region of Interest) based secondary analysis.

This atlas is freely available online for public access.

2. Materials and methods

2.1. Specimen preparation

Five 6-month old female pigs (*Sus scrofa domesticus*) of 31 kg mean live weight and 88 g mean brain weight were used for this work. Animals were obtained from a local inbreeding between French Landrace × Large White females and Piétrain males.

The animals were sacrificed under deep anesthesia using a 500 mg I.V. dose of pentobarbital. After decapitation, the heads were perfused via the carotid artery with 5 L of 4% paraformaldehyde (PFA 4%) in 0.15 M phosphate buffer for approximately 25 min. The brains were extracted from the skull and stored in the fixative (PFA, 4%) for 14 days.

All experimental procedures were carried out according to guidelines for the care and use of animals approved by the French Animal Experiments Inspectorate.

2.2. MR image acquisition

Before imaging, the brains were removed from the formalin fixative and immersed in fomblin (perfluoropolyether, Ausimont, Morristown, NJ, USA) for 60 min. Immersion eliminates the majority of air bubbles from the exterior and various crevices of the brain. Each brain was positioned within a 72 mm diameter radio frequency (RF) coil's internal chamber and placed in the magnet bore. MR images were acquired on a BIOSPEC 47/40 4.7 T MRI system (Bruker, Germany) equipped with a 400 mT m^{-1} shielded gradient insert. The parameters used to acquire MRI data were as follows: three-dimensional gradient-echo sequence with an acquisition bandwidth of 25 kHz, TR/TE = 40.6/20 ms, 40° flip angle, 8 averages, a field of view of 64.0 mm × 51.2 mm × 78.4 mm and an acquisition matrix of 640 × 512 × 256, leading to a 100 μm × 100 μm × 306 μm voxel resolution in 8 h 42 min. Image reconstruction using a 3D fast-Fourier transform was performed using the Bruker ParaVision software v4.02.

2.3. Brain processing

We used the methodology described by Yelnik et al. for human brain histological atlas construction (Yelnik et al., 2007). Briefly, after MR imaging, each brain was immersed in a 30% sucrose solution for 8 days at 4 °C. Once it had sunk to the bottom of the recipient, the brain was removed and separated into two hemispheres along the midsagittal plane.

Each hemisphere was cut into three 1 cm-thick blocks oriented in the sagittal plane parallel to the anterior commissural (ac) and posterior commissural (pc) line. The blocks were deposited on a 3 mm cork support before being embedded in a 7% gelatin solution and frozen at constant −75 °C using the tissue freezing system SnapFrost® (Alphelys – France). The frozen blocks were cut into 70-μm-thick sections on a freezing microtome every 350 μm. The histological sections obtained for each hemisphere were collected serially into numbered boxes. Each section was thus parallel to the ac–pc axis and able to be located precisely along the right–left axis (*X*-axis) of the brain. For each hemisphere, sections presenting the fewest artifacts were stained for Nissl substance (cresyl-violet).

2.4. Atlas construction

The construction of the atlas was similarly generated from histological and MR images.

To minimize both extraction and fixation artifacts, we opted for the construction of a virtual symmetrical brain obtained from one of the ten initial hemispheres selected on the basis of its high grey–white quality contrast. These MR images and their corresponding available histological images were reoriented along the anterior and posterior commissure (ac–pc) in the midsagittal plane and then symmetrized, leading to a virtual MR and histological volume. After histological analysis which enabled microscopic cortical and subcortical structure delineation, coregistration of the histological images and T2-weighted MRI was performed using the MRI atlas as the standard stereotaxic space.

Finally a manual segmentation step allowed construction of 3D anatomical volumes of interest for each individual brain structure.

2.4.1. T2-weighted 4.7 T MR image processing

The MRI images corresponding to the selected hemisphere were separated from the ipsilateral hemisphere's images using 3D Slicer Software. The remaining images were perfectly reoriented along the ac–pc axis and then symmetrized through the midsagittal plane, yielding a virtual 3D MRI atlas.

2.4.2. Histological image acquisition and processing

82 Cresyl-violet-stained sagittal sections corresponding to the selected hemisphere were scanned using high-resolution settings (500 ppi). Background was automatically removed using Image J software. Each histological image was automatically registered to its neighboring image using BrainVISA/Anatomist Software (Cointepas et al., 2001).

The histological sections were analyzed under low-power field (×20 to ×44) on a Nikon SMZ645A binocular. The boundaries of 30 deep cerebral structures were traced with a mouse and cursor on a live video image of the 82 sagittal sections using Adobe Photoshop CS Extended.

A high-power microscopic examination (×100 and ×200) was also performed on a Nikon Eclipse E400. This step allowed cytoarchitectonic brain mapping according to Brodmann's neuronal laminar organization into six layers for the neocortex and less than six layers for the archicortex (Brodmann, 1909).

After microscopic examination, the 82 histological images were duplicated and underwent symmetrical construction according to the midsagittal plane before being stacked on Image J, yielding a three-dimensional histological atlas (Fig. 1).

2.4.3. Coregistration of histological and MRI atlas

The histological volume of the brain was warped to the undistorted MR volume of the same brain using rigid transformations. The rigid transformation was performed on 3D Slicer Software using two fiducial landmarks: the center of the ac and the bottom edge of the bend of the pc. The distortion during sample histological processing and the consequent lack of accurate 3D information particularly in cortical areas make it hard to apply affine and elastic transformations and to expect conclusive results.

2.4.4. Manual segmentation

Coregistration of the histological and MR atlases enabled comparison of all the delineations achieved on the histological slides when necessary on MR images (Fig. 2).

The 4.7 T brain MR images yielded high cortex-to-background noise contrast on the T2-weighted images, and this made it possible

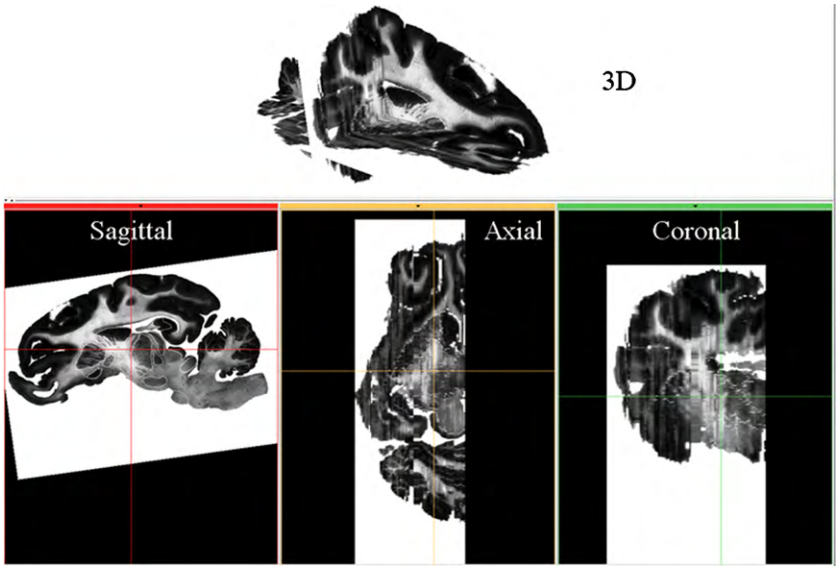

Fig. 1. 3D view of the histological atlas after automatic registration of each image to its neighbouring one and after histological volume warping to the undistorted MR volume of the same hemisphere using rigid transformations. The sagittal plane was the reference plane and allowed microscopic delineation of cortical and subcortical areas.

to segment a majority of cerebral structures easily without using histological control. Indeed, the histological study only appeared necessary for refining recognition of the thalamic nuclei as well as the exact demarcation of the posterior limit of the hippocampus, the anterior and inferior limit of the caudate nucleus and its exact bounds with the nucleus accumbens. A histological low-power magnification analysis was also particularly crucial for hypothalamic nuclei recognition.

The MR hemisphere images were segmented manually into 104 volumes of interest (VOI) including 53 deep brain nuclei and structures, 5 ventricular system areas, 6 deep cerebellar nuclei, 12 cerebellar lobules and 28 cortical areas. The symmetrization step led to 178 individual VOI in the entire atlas. English labels and corresponding abbreviations in the atlas are in accordance with reference works (Mai et al., 2004; Paxinos and Watson, 2007) and are reported in Table 1.

All identified regions were traced and labeled manually using 3D Slicer software (Massachusetts Institute of Technology, USA) (Gering et al., 1999). Because the contrast of one structure against the background was not the same on the three different views (coronal, sagittal and axial), delineation of each structure was systematically carried out using the three views. Segmentation tools in 3D Slicer software, such as interpolation and automatic label smoothing, were used.

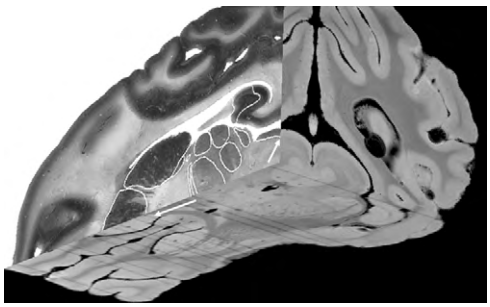

Fig. 2. Coregistration of histological sections and MR images. In this 3D view, the sagittal plane is a Nissl section and the axial and coronal planes are MR images. Note the good correspondence of putamen (forward) and superior colliculus (backward) pointed by white arrows.

3. Results

We developed an MRI digital atlas in which 178 cerebral and cerebellar structures were identified (Table 1). The usual brain extraction artifacts, such as cerebellar flocculus, pineal gland and olfactory bulb shifts, were overcome with the construction of a virtual symmetrical brain in which many of these extraction biases have been attenuated. Some minor cortical cracks and air bubbles are still present.

3.1. Deep brain structure analysis

The high quality of the MR and histological images enabled easy individualization of the 53 deep brain nuclei and structures reported in Table 1.

The segmentation step allowed subdivision of the thalamus into nine distinct nuclei (AV, CTA, MD, LD, G, Pul, Rt, VA, VP). Five distinct structures were individualized in the striate system (Acb, Cd, Cl, GP, Pu, SN). Four structures were individualized in the limbic system (fx, Hi, S, A). The subiculum, which represents the junction between the entorhinal gyrus (area 34 in Brodmann's mapping system) and CA1, was clearly identifiable on the studied images and thus was individualized in the atlas (Fig. 3). The hippocampus included 5 histological areas: dentate gyrus, CA1, CA2, CA3 and CA4 (Fig. 3). Two subthalamic (STh, ZI) and two epithalamic structures (Hb, Pi) were also individualized with a notable displacement artifact for the pineal gland.

The histological sections allowed delineation of 3 distinct hypothalamic areas (AH, MB, MH). 13 cerebral trunk structures were individualized: 6 in the mesencephalon (IC, SC, PAG, R, OT, PTc), 3 in the pons (IP, Pn, RFTg) and 4 in the medulla oblongata (Cu, Sol, Ol, SOC). Only six cranial nerve nuclei (5, 6, 7, 8, 10 and 12) were clearly identified and reported in the atlas. Trigemini nervi were subdivided into 3 structures (Mo5, Sp5, sp5).

Four major median white matter anatomical structures were also individualized in the atlas (cc, ox, ac, pc). The latter two structures represent the major fiducial points used in manual coregistration of the atlas.

The ventricular system was individualized in the two lateral ventricles (left and right LV), the third ventricle (3V), and the fourth ventricle (4V) with overprecision for the cerebral aqueduct (Aq).

Table 1
Index of structures with corresponding label number and abbreviation.

No.	Structure	Abb	No.	Structure	Abb
	Central structures			Deep cerebellar structures	
	Thalamus		160;161	Lateral cerebellar nucleus	Lat
5;6	Anteroventral thalamic nucleus	AV	162;163	Medial cerebellar nucleus	Med
7;8	Central thalamic area	CTA	164;165	Interposed cerebellar nucleus	Int
9;10	Mediodorsal thalamic nucleus	MD	166;167	Inferior cerebellar peduncle	ICP
11;12	Laterodorsal thalamic nucleus	LD	168;169	Medial cerebellar peduncle	MCP
13;14	Geniculate nuclei	G	170;171	Superior cerebellar peduncle	SCP
15;16	Pulvinar nuclei	Pul			
17;18	Reticular thalamic nucleus	Rt		Cerebellar lobules	
19;20	Ventral anterior thalamic nucleus	VA	181	Cerebellar lobule I,II	I,II
21;22	Ventral posterior thalamic nucleus	VP	183	Cerebellar lobule III	III
	Striate system		184	Cerebellar lobule IV	IV
23;24	Accumbens nucleus	Acb	185	Cerebellar lobule V	V
25;26	Caudate nucleus	Cd	186	Cerebellar lobule VI	VI
27;28	Claustrum	Cl	191	Crus1 of the ansiform lobule	Crus1
29;30	Globus pallidus	GP	192	Crus2 of the ansiform lobule	Crus2
31;32	Putamen	Pu	187	Cerebellar lobule VIIB	VIIB
33;34	Substantia nigra	SN	188	Cerebellar lobule VIIIA	VIIIA
	Limbic system		193	Cerebellar lobule VIIIB	VIIIB
35	Fornix	fx	189	Cerebellar lobule IX	IX
36;37	Hippocampus	Hi	190	Cerebellar lobule X	X
38;39	Subiculum	S			
40;41	Amygdala	A		Brodmann's area	
	Subthalamus		101;201	Primary somatosensory cortex	Area 1,2,3
42;43	Subthalamic nucleus	STh	104;204	Primary motor cortex	Area 4
44;45	Zona incerta	ZI	105;205	Somatosensory association cortex	Area 5-7
	Epithalamus		106;206	Premotor cortex	Area 6
46;47	Habenular nuclei	Hb	109;209	Dorsolateral prefrontal cortex	Area 9
48	Pineal gland	Pi	110;210	Anterior prefrontal cortex	Area 10
	Hypothalamus		111;211	Orbitofrontal cortex	Area 11
49;50	Anterior hypothalamic area	AH	113;213	Insular cortex	Area 13,14
51	Mamillary body	MB	117;217	Primary visual cortex (V1)	Area 17
52;53	Medial hypothalamic area	MH	118;218	Secondary visual cortex (V2)	Area 18
	Mesencephalon		119;219	Associative visual cortex (V3)	Area 19
54;55	Inferior colliculus	IC	120;220	Inferior temporal gyrus	Area 20
56;57	Superior colliculus	SC	121;221	Middle temporal gyrus	Area 21
58	Periaqueductal gray	PAG	122;222	Superior temporal gyrus	Area 22
59;60	Red nucleus	R	123;223	Ventral posterior cingulate cortex	Area 23
61;62	Nucleus of the optic tract	OT	124;224	Ventral anterior cingulate cortex	Area 24
63;64	Pretectal area	PTc	126;226	Ectosplenial area	Area 26
	Pons		127;227	Piriform cortex	Area 27
65	Interpeduncular nucleus	IP	129;229	Retrosplenial cingular cortex	Area 29
66;67	Pontine nuclei	Pn	131;231	Dorsal posterior cingular cortex	Area 31
68;69	Reticulotegmental nucleus of the pons	RFTg	132;232	Dorsal anterior cingulate cortex	Area 32
	Medulla oblongata		134;234	Anterior entorhinal cortex	Area 34
70;71	Cuneate nucleus	Cu	135;235	Perirhinal cortex	Area 35
72;73	Nucleus of the solitary tract	Sol	136;236	Parahippocampal cortex	Area 36
74;75	Olivary nuclei	Ol	137;237	Fusiform gyrus	Area 37
76;77	Superior olivary complex	SOC	141;142	Auditory cortex	Area 41-42
	Cranial nerves		149;249	Prepiriform area	Area 49
78;79	Dorsal motor nucleus of vagus	10	151;251	Olfactory bulb	Area 51
80;81	Motor trigeminal nucleus	Mo5			
82;83	Spinal trigeminal nucleus	Sp5			
84;85	Abducens nucleus	6		Ventricular system	
86;87	Facial nucleus	7	94,95	Lateral ventricle	LV
88;89	Hypoglossal nucleus	12	96	Third ventricle	3V
90;91	Spinal trigeminal tract	sp5	97	Fourth ventricle	4V
92;93	Vestibular nucleus	Ve	98	Cerebral aqueduct (Sylvius)	Aq
	Other				
2	Anterior commissure	ac			
4	Corpus callosum	cc			
3	Optic chiasm	ox			
1	Posterior commissure	pc			

Paired cerebral and cerebellar structures have two label numbers: odd numbers are for left hemisphere and even numbers are for right hemisphere. Numbers 101–151 correspond to the left hemisphere Brodmann's area and numbers 201–251 correspond to the right hemisphere Brodmann's area.

3.2. Cytoarchitectonic study

Microscopic analysis of the histological slices allowed recognition of 25 neocortical areas and 3 paleocortical areas which were reported on the corresponding MR images during the manual segmentation step (Table 1).

Cortical areas were subdivised into prefrontal, motor cortex, somatosensory cortex, auditory cortex, visual cortex, cingulate cortex and limbic cortex.

The prefrontal cortex includes Brodmann's areas 8–11, 14–16, 24, 32 and 47. These areas are respectively grouped into the frontopolar region (areas 8–11), anterior cingulate cortex (areas 24

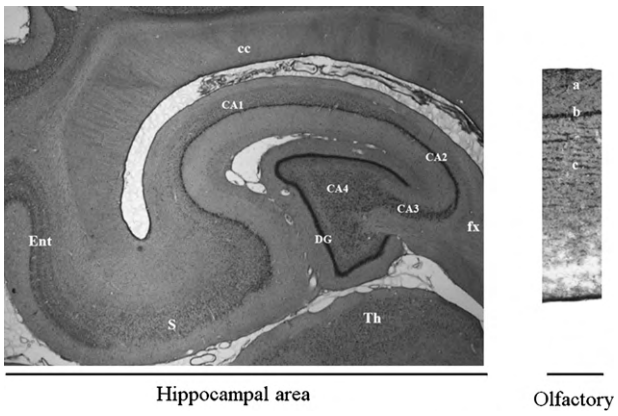

Fig. 3. Cytoarchitectonic delineations of the archicortical and the paleocortical areas of the domestic pig brain. These areas correspond to the hippocampal area for the archicortex and to the olfactory system for the paleocortex and do not present the classical cortical subdivision into six layers. Hippocampal area includes both hippocampus and subiculum (S). Hippocampus is subdivided in dentate gyrus (DG), and the areas CA1 to CA4. Hippocampus is separated from the entorhinal cortex (Ent) by the subiculum (S). Entorhinal cortex corresponds to area 34 in Brodmann's cortical mapping. Hippocampus is located beneath the corpus callosum (cc), behind the fornix (fx) and above the thalamus (Th). Olfactory bulb is subdivided in 3 distinct layers from surface to depth: the glomerular layer (a), the mitral cell layer (b), and the granule cell layer (c).

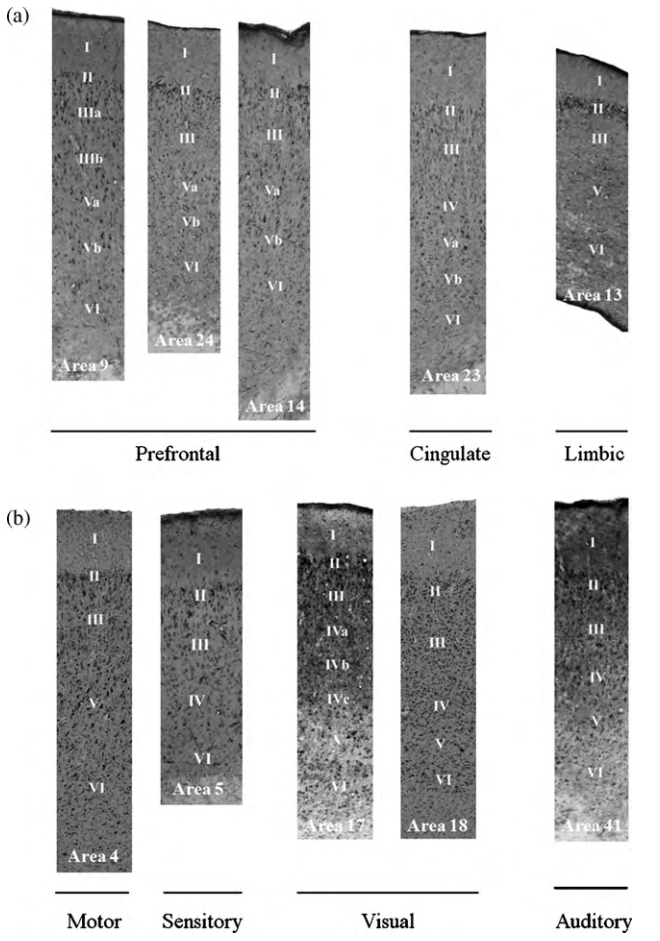

Fig. 4. Cytoarchitectonic delineations of major cortical areas of the domestic pig brain in prefrontal, cingulate, limbic, motor, sensitory, visual and auditory cortex. Specific aspects in the 6 layers lamination allowed their recognition on microscopic analysis (cresyl-violet stain, magnification ×40). Prefrontal cortex is agranular (lack layer IV). Motor cortex presents a large layer V. Primary visual area (area 17) owns a large layer IV visible at low magnification.

and 32), anterior insular cortex (areas 14–16) and the dorsofrontal region (area 47) in Okada's terminology (Okada et al. 1999) and in recent reference publications (Jelsing et al., 2006).

The prefrontal cortex is agranular, and thus lacks a granular layer IV. Infragranular layer V is divided into an upper (Va) and lower (Vb) less cell-dense layer (Fig. 4).

The motor cortex includes Brodmann's areas 4 and 6. These agranular areas are distinguished by a less cell-dense layer III and the presence of large pyramidal neurons in layer V. Area 4 can be distinguished by the presence of Betz giant cells that do not appear in area 6 (Fig. 4).

The somatosensory cortex includes areas 1, 2, 3, 5 and 7 in Brodmann's cortical segmentation. These areas present a large layer V with large pyramidal cells. The infragranular layers present low cellular density and layer IV appears thick (Fig. 4).

The visual cortex covers the occipital region. It includes areas 17, 18 and 19. Area 17 is characterized by the division of layer IV into three sublayers (IVa, IVb and IVc). Areas 18 and 19 surround area 17 (Fig. 4).

The auditory cortex belongs to the temporal region. It includes areas 21, 22, 41 and 42. These areas present large granular layers (Fig. 4).

The insular cortex includes 2 separate parts, one posterior and granular (area 13) and the other anterior and agranular (areas 14–16) which belong to the prefrontal cortex (Fig. 4).

The cingulate region borders the corpus callosum. It has two distinct parts: the postcingulate subregion and the precingulate subregion. The precingulate subregion is agranular and corresponds to the anterior cingulate cortex which belongs to the prefrontal cortex. It includes Brodmann's areas 24 and 32. The postcingulate subregion has a distinct inner granular layer (Fig. 4). It includes Brodmann's areas 23 and 31.

The hippocampal region includes the hippocampus and subiculum which belong to the archicortex and areas 34 and 35, which follows the subiculum and belongs to the neocortex. Area 35 appears clearly laminated compared to area 34 (Fig. 3).

We also identified 3 paleocortical areas belonging to the olfactory system: area 27 (piriform cortex), area 49 (prepiriform area) and area 51 (olfactory bulb). These paleocortical areas are formed from basic cortical structures of which the laminar pattern is relatively atypical and cannot be traced back to the primitive cortical type. A type of layers I, II and VI, also called glomerular layer, mitral cell layer and granule cell layer, can be distinguished (Fig. 3).

3.3. Cerebellar study

MR image and histological slide analysis allowed identification of 6 cerebellar nuclei (Table 1): L, M, NIC, PCI, PCM, PCS. The advantage of three-dimensional visualization by 3D Slicer also facilitated the identification of 13 cerebellar fissures and lobules according to the Schmahmann classification (Schmahmann et al., 1999): cerebellar lobules I to VI, VIIB, VIIIA, VIIIB, IX, X, and Crus1 and Crus2.

3.4. Atlas data availability

The corresponding 3D histological atlas (Fig. 1) has helped us to complete the missing or poorly defined structures in the MR image segmentation step and to establish accurate cortical mapping (Fig. 2). The 3D digital atlas allows full orthogonal display of a single brain specimen with easy visualization of histological and MR images. The digital volume may also be resampled in any plane, allowing reference to any coordinate system and investigation through any region of interest. More advanced visualization

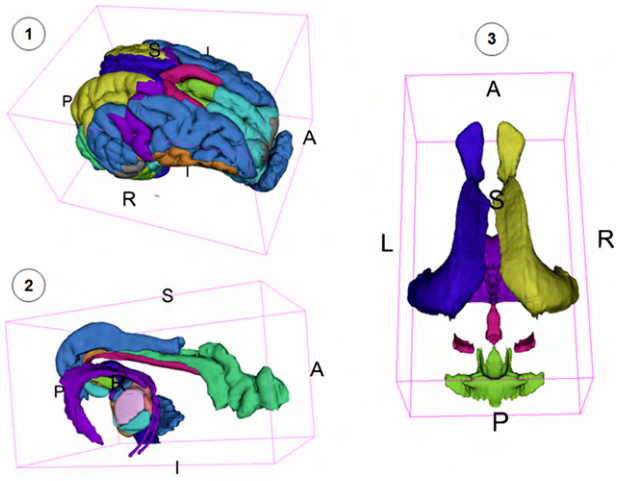

Fig. 5. Illustration of some anatomical spatial view examples provided by the atlas: 1 – lateral view of the cortical areas, 2 – lateral view of the limbic system, 3 – upper view of the cerebral ventricles. Boundaries of the box allow an easy spatial orientation: A–P (anterior–posterior), R–L (right–left), S–I (superior–inferior).

in three dimensions is obtained from surface renderings of individual segmented structures and allows easy comprehension of anatomical structures (Fig. 5).

All the atlas data and a brief tutorial explaining how to visualize the atlas are available on our institution's website (http://www.rennes.inra.fr/senah/brain_atlas). Data are available in Nifti format and can be browsed easily in 3D Slicer and MRICron according to the wishes or habits of the user. These software packages allow the users to browse and visualize the digital atlas slice-by-slice in three orthogonal views. The *X*-axis corresponds to the mediolateral axis (positive values for the right side), the *Y*-axis corresponds to the rostrocaudal axis (positive values for the anterior side) and the *Z*-axis corresponds to the dorsoventral axis (positive values for the dorsal side). Data are provided in a reference frame defined by the ac–pc axis in the midsagittal plane with the bottom part of the bend of the pc as the zero reference point.

4. Discussion

The purpose of this work was to obtain a pig brain atlas enabling overall atlas-to-atlas registration, trajectory planning, and targeting of cortical areas. This atlas may also serve as a global positioning system which can counterbalance the lack of resolution of the pig brain images usually obtained and in which the numerous deep cerebral structures are often hardly identifiable.

The high quality of the signal obtained with 4.7 T MRI yielded a satisfactory delineation of a large number of subcortical structures. Cryosectioned histological image analysis allowed more precise determination of the boundaries of a few subcortical structures (some thalamic nuclei and hypothalamic areas) and the cortical parcellation according to Brodmann's classification.

Parcellation refers to subdivision of the atlas into homogenous regions currently with three possible levels of atlas parcellation: low, medium, and high. Low parcellation means fewer atlas structures than discernible in a corresponding structural scan; medium parcellation is comparable to (or slightly better than) that of a structural scan; and high parcellation provides far more details than the corresponding structural scan (Nowinski, 2008). In our atlas, the majority of identified structures were clearly visualized on MR images and were of medium parcellation level. A few structures whose volume did not generally exceed 5 mm^3 were not detailed in the atlas and were considered as low parcellated structures. This was the case of some cranial nerve nuclei. On the other hand, subdivision of some thalamic and hypothalamic nuclei according to Brodmann's area recognition was enabled by histological slide analysis and considered to be of the high parcellated type.

4.1. Deep brain structure analysis

The deep cerebral structures identified in this atlas were compared to the few pig brain atlases available in the literature (Felix et al., 1999; Salinas-Zeballos et al., 1986; Watanabe et al., 2001; Yoshikawa, 1968) in addition to the studies on specific subcortical areas such as the hypothalamus (Ettrup et al., 2010), the substantia nigra (Nielsen et al., 2009) and the subthalamic nucleus (Larsen et al., 2004). The sole valid source of comparison was represented by Felix's stereotaxic adult domestic pig brain atlas (Felix et al., 1999). This comparison revealed an overall shift of 2–3 mm in the *X*, *Y* and/or *Z*-axis in relation to our stereotaxic coordinates, which can be explained by differences in the construction of these two atlases. Indeed, Félix's atlas was constructed from in vivo brains with external landmarks whereas our atlas was constructed from an ex vivo brain with the ac–pc axis as the internal landmark.

Another difference noted with Félix's atlas concerns some central structures which appeared to be subdivided into more nuclei than ours. These nuclei include the habenular nuclei (Hb), for which a lateral and medial subdivision is individualized in Felix's atlas, whereas we distinguished a sole structure in our atlas. This was also the case for the geniculate nuclei (G) with a lateral and medial subdivision in the Felix atlas, for the mamillary body (MB) with anterior, medial and lateral subdivision, and for the substantia nigra with a distinction between the pars compacta and pars reticulata. The thalamic nuclei are also more detailed in the Felix atlas with 13 identified structures compared to 6 in our atlas (Table 2).

These supplementary subdivisions observed in Felix's atlas provide more anatomical details and greater analogy with the corresponding structures observed in the human brain but could not be clearly identified on both our MR and histological images. Considering the small size of these structures, making individualized

Table 2
Annotation of the differences between Felix's atlas and present atlas.

Felix atlas	Present atlas	Name	Abbreviation
HM	Hb	Habenular nuclei	Hb
HL		Medial habenular nucleus	HM
		Lateral habenular nucleus	HL
GM	NG	Geniculate nuclei	G
GL		Medial geniculate nucleus	GM
		Lateral geniculate nucleus	GL
MA	MB	Mamillary body	MB
MM		Anterior mamillary area	MA
ML		Medial mamillary nucleus	MM
		Lateral mamillary nucleus	ML
Snc	SN	Substantia nigra	SN
Snr		Substantia nigra, pars compacta	Snc
		Substantia nigra, reticular part	Snr
AD		Anterodorsal thalamic nucleus	AD
AM	AV	Anteromedial thalamic nucleus	AM
AV		Anteroventral thalamic nucleus	AV
CM		Central thalamic area	CTA
CD	CTA	Central medial thalamic nucleus	CM
CL		Circular nucleus	CD
		Centrolateral thalamic nucleus	CL
DM	MD	Mediodorsal thalamic nucleus	MD
LD	LD	Laterodorsal thalamic nucleus	LD
LP		Lateral posterior thalamic nucleus	LP
VA	VA	Ventral anterior thalamic nucleus	VA
VL		Ventrolateral thalamic nucleus	VL
VM	VP	Ventromedial thalamic nucleus	VM
VP		Ventral posterior thalamic nucleus	VP

imaging impossible, we did not feel it erroneous to group them into larger structures in our results.

4.2. Cytoarchitectonic study

The microscopic examination of the cytoarchitectonic cortical ribbon allowed us to identify, in relation to the sulci and gyri, 33 cortical areas (or Brodmann's areas). Areas 15, 25, 28, 30, 33, 38, 43, 46 and 48 were not clearly identified. Area 51, corresponding to the olfactory bulb, has no equivalent in the human brain. Some boundaries between two areas were not clearly defined on the histological slides and were refined by the three-dimensional segmentation of the MR images.

A few cortical maps of the entire neocortex are available (Campbell, 1905; Kruska, 1970; Stephan, 1951) in addition to some studies on specific cortical regions such as the prefrontal cortex (Jelsing et al., 2006), motor cortex (Breazile et al., 1966), somatosensory cortex (Craner and Ray, 1991a,b; Okada et al., 1999), auditory cortex (Andrews et al., 1990; Plogmann and Kruska, 1990), occipital cortex (Fang et al., 2006; Kruska, 1972), and allocortex (Holm and West, 1994; Kruska and Stephan, 1973).

Within the limits of a proper comparison with our work, these studies do not seem to contradict our results. They nevertheless demonstrate the difficulty involved in the spatial assessment of the cortical areas on 2D drawings and the full advantages of 3D visualization in the understanding of the spatial distribution of cortical areas.

However it must be keep in mind that our results, although covering the entire cortical ribbon, are obtained from the single cytoarchitectural study and for this reason can only be approximate. Further confirmation by electrophysiological mapping (Okada et al., 1999), anterograde or retrograde tracing studies (Jelsing et al., 2006) and functional imaging studies (Cumming et al., 2007) are highly recommended to validate our mapping technique.

4.3. Cerebellar study

The identification of 6 cerebellar nuclei was achieved without any major problem of demarcation on our MR images (Table 1). The advantage of the three-dimensional visualization by 3D Slicer also facilitated identification of 13 cerebellar fissures and lobules according to the classification of Schmahmann et al. (1999) which corresponds to a revised version of the Larsell's nomenclature (Larsell and Jansen, 1972). Nevertheless, with the exception of the proportionally smaller size of these fissures and lobules in the pig cerebellum in relation to the human cerebellum, we managed to identify them easily.

4.4. Atlas data availability

This atlas provides the key attributes generally required for atlas construction (McLaren et al., 2009; Van Essen and Dierker, 2007). It presents high spatial resolution, identifies cortical areas, provides a standard coordinate space, can be linked to future digital intra- or inter-species atlases, is readily accessible and easily visualized. It can also be extensible and linked to a database for experimental data.

This atlas is a combined histology and high-resolution MRI atlas of a domestic pig brain offering an accompanying set of histological sections and VOI of the cytoarchitectural and subcortical structures for each 0.15 mm MRI slice.

The major interest of this digital atlas is that it provides a common standardized space allowing future studies from different institutions to report their findings in the same coordinate system analogous to the use of a standardized space in humans such as MNI (Mazziotta et al., 2001).

In current usage, this atlas has demonstrated its reliability in the establishment of a probabilistic atlas of deep brain nuclei and the creation of a population-average atlas of a domestic pig. These two studies are being carried out in parallel in our institution (data not shown). In these trials, the atlas allowed easy coregistration with in vivo 1.5 T MR brain images requiring only rigid transformations.

Although we have not done so, it should be possible to relate the brain-based coordinate system to a skull-based system so that the atlas could be used as a guide for positioning recording electrodes or pipettes for injections of tracers.

Finally, it seems necessary in future studies to validate the atlas on the brains of other pig species as deep brain structure size differences may be correctable by global scaling (Bowden and Dubach, 2000). However, this is less the case for sulcal pattern variations which require species-specific atlases as these cannot be easily corrected (Van Der Gucht et al., 2006).

5. Conclusion

With the help of high-resolution MR and histological Image 3D construction for one hemisphere, we developed a detailed digital, three-dimensional atlas of the domestic pig. The digital volume may be resampled in any plane, allowing reference to any coordinate system and investigation through any region of interest. This atlas can be used as a standard stereotaxic space and can facilitate anatomical identification in cerebral imaging and automatic segmentation for future brain studies.

References

Andrews RJ, Knight RT, Kirby RP. Evoked potential mapping of auditory and somatosensory cortices in the miniature swine. Neurosci Lett 1990;114:27–31.
Bowden D, Dubach MF. Applicability of the template atlas to various primate species. In: Martin R, Bowden DM, editors. Primate brain maps: structure of the macaque brain. New York: Elsevier; 2000.
Breazile JE, Swafford BC, Thomson WD. Study of the motor cortex of the domestic pig. Am J Vet Res 1966;27:1369–73.
Brodmann K. Vergleichende Lokalisationslehre der Grosshirnrinde in ihren Prinzipien dargestellt auf Grund des Zellenbaues, Barth Leipzig. In: Some papers on the cerebral cortex translated as: on the comparative localization of the F cortex. Springfield, IL: Thomas; 1909. pp. 201–230.
Campbell AW. Histological studies on the localisation of cerebral function. Cambridge: Cambridge University Press; 1905.
Cointepas Y, Mangin JF, Garnero L, Polinet JB, Benali H. BrainVISA: software platform for visualization and analysis of multi-modality brain data. Neuroimage 2001;13:98.
Craner SL, Ray RH. Somatosensory cortex of the neonatal pig: I. Topographic organization of the primary somatosensory cortex (SI). J Comp Neurol 1991a;306:24–38.
Craner SL, Ray RH. Somatosensory cortex of the neonatal pig: II. Topographic organization of the secondary somatosensory cortex (SII). J Comp Neurol 1991b;306:39–48.
Cumming P, Møller M, Benda K, Minuzzi L, Jakobsen S, Jensen SB, et al. A PET study of effects of chronic 3,4-Methylenedioxymethamphetamine (MDMA, "Ecstasy") on serotonin markers in Gottingen minipig brain. Synapse 2007;61:478–87.
Ettrup KS, Sørensen JC, Bjarkam CR. The anatomy of the Göttingen minipig hypothalamus. J Chem Neuroanat 2010;39(3):151–65.
Fang M, Li J, Rudd JA, Wai SM, Yew JC, Yew DT. fMRI mapping of cortical centers following visual stimulation in postnatal pigs of different ages. Life Sci 2006;78:1197–201.
Felix B, Leger ME, Albe-Fessard D. Stereotaxic atlas of the pig brain. Brain Res Bull 1999;49:1–138.
Gering D, Nabavi A, Kikinis R, Grimson WEL, Hata N, Everett R, et al. An integrated visualization system for surgical planning and guidance using image fusion and interventional imaging. In: Medical image computing and computer-assisted intervention (MICCAI); 1999.
Holm IE, West MJ. Hippocampus of the domestic pig: a stereological study of subdivisional volumes and neuron numbers. Hippocampus 1994;4:115–25.
Jelsing J, Hay-Schmidt A, Dyrby T, Hemmingsen R, Uylings HBM, Pakkenberg B. The prefrontal cortex in the Göttingen minipig brain defined by neuronal projection criteria and cytoarchitecture. Brain Res Bull 2006;70:322–36.
Kruska D. Comparative cytoarchitectonic investigations in brains of wild and domestic pigs. Z Anat Entwicklungsgesch 1970;131:291–324.
Kruska D. Volumetric comparison of various visual centers in the brains of wild boars and domestic pigs. Z Anat Entwicklungsgesch 1972;138:265–82.
Kruska D, Stephan H. Volumetric comparison of allocortical brain centers in wild and domestic pigs. Acta Anat 1973;84:387–415.

Larsell O, Jansen J. The comparative anatomy and histology of the cerebellum. The human cerebellum, cerebellar connections, and cerebellar cortex. Minneapolis: Univ. Minnesota Press; 1972.
Larsen M, Bjarkam CR, Østergaard K, West MJ, Sørensen JC. The anatomy of the porcine subthalamic nucleus evaluated with immunohistochemistry and design-based stereology. Anat Embryol 2004;3:239–47.
Lind NM, Moustgaard A, Jelsing J, Vajta G, Cumming P, Hansen AK. The use of pigs in neuroscience: modeling brain disorders. Neurosci Biobehav Rev 2007;31:728–51.
Mai JK, Assheuer J, Paxinos G. Atlas of the human brain. London: Elsevier Academic Press; 2004.
Malbert CH, Horowitz M. The pig as a model for human digestive motor activity. In: Laplace JP, Février C, Barbeau A, editors. Digestive physiology in pigs. Paris: EAAP Publication; 1997. p. 3–13.
Mazziotta JC, Toga A, Evans AC, Fox P, Lancaster J, Zilles K, et al. A probabilistic atlas and reference system for the human bra International Consortium for Brain Mapping (ICBM). Phil Trans R Soc Lond B 2001;356:1293–322.
McLaren DG, Kosmatka KJ, Oakes TR, Kroenke CD, Kohana SG, Matochik JA, et al. A population-average MRI-based atlas collection of the rhesus macaque. Neuroimage 2009;45:52–9.
Nielsen MS, Sørensen JC, Bjarkam CR. The substantia nigra pars compacta of the Göttingen minipig: an anatomical and stereological study. Brain Struct Funct 2009;213:481–8.
Nowinski WL. Towards construction of an ideal stereotactic brain atlas. Acta Neurochir 2008;150:1–14.
Okada Y, Lahteenmaki A, Xu C. Comparison of MEG and EEG on the basis of somatic evoked responses elicited by stimulation of the snout in the juvenile swine. Clin Neurophysiol 1999;110:214–29.
Paxinos G, Watson C. The rat brain in stereotaxic coordinates. London: Academic Press; 2007.
Plogmann D, Kruska D. Volumetric comparison of auditory structures in the brains of European wild boars (*Sus scrofa*) and domestic pigs (*Sus scrofa f. dom*). Brain Behav Evol 1990;35:146–55.
Salinas-Zeballos ME, Zeballos GA, Gootman PM. A stereotaxic atlas of the developing swine (Sus scrofa) forebrain. In: Tumbleson ME, editor. Swine in biomedical research. New York: Plenum Press; 1986. p. 887–906.
Sauleau P, Lapouble E, Val-Laillet D, Malbert CH. The pig model in brain imaging and neurosurgery. Animal 2009;3:1138–51.
Schmahmann JD, Doyon J, McDonald D, Holmes C, Lavoie K, Hurwitz AS, et al. Three-dimensional MRI atlas of the human cerebellum in proportional stereotaxic space. Neuroimage 1999;10:233–60.
Spurlock ME, Gabler NK. The development of porcine models of obesity and the metabolic syndrome. J Nutr 2008;138:397–402.
Stephan H. Vergleichende Untersuchungen über Feinbau des Hirnes von Wild- und Haustieren. Zool Jahrb Abt Anat Ontog Tiere 1951;71:487–586.
Van Der Gucht E, Youakim M, Arckens L, Hof PR, Baizer JS. Variations in the structure of the prelunate gyrus in Old World monkeys. Anat Rec A Discov Mol Cell Evol Biol 2006;288:753–75.
Van Essen DC, Dierker DL. Surface-based and probabilistic atlases of primate cerebral cortex. Neuron 2007;56:209–25.
Watanabe H, Andersen F, Simonsen CZ, Evans SM, Gjedde A, Cumming P, DaNeX Study Group. MR-based statistical atlas of the Göttingen minipig brain. Neuroimage 2001;14:1089–96.
Yelnik J, Bardinet E, Dormont D, Malandain G, Ourselin S, Tandé D, et al. A three dimensional, histological and deformable atlas of the human basal ganglia. I. Atlas construction based on immunohistochemical and MRI data. NeuroImage 2007;34(2):618–38.
Yoshikawa T. The brain of the pig (Yorkshire breed).Atlas of the brains of domestic animals, 1st ed. Tokyo and University Park: Univ. of Tokyo Press and Pennsylvania State Univ.; 1968.